

PAPER

Weight Optimization for Multiple Image Integration and Its Applications*

Ryo MATSUOKA[†], *Student Member*, Tomohiro YAMAUCHI[†], *Nonmember*, Tatsuya BABA[†], *Student Member*, and Masahiro OKUDA[†], *Member*

SUMMARY We propose an image restoration technique that uses multiple image integration. The detail of the dark area when acquiring a dark scene is often deteriorated by sensor noise. Simple image integration inherently has the capability of reducing random noises, but it is especially insufficient in scenes that have a dark area. We introduce a novel image integration technique that optimizes the weights for the integration. We find the optimal weight map by solving a convex optimization problem for the weight optimization. Additionally, we apply the proposed weight optimization scheme to a single-image super-resolution problem, where we slightly modify the weight optimization problem to estimate the high-resolution image from a single low-resolution one. We use some of our experimental results to show that the weight optimization significantly improves the denoising and super-resolution performances.

Key words: denoising, convex optimization, high dynamic range images, super-resolution

1. Introduction

A high ISO sensitivity setting is required when taking photographs with a hand-held camera under a dark lighting condition to restore the dark area without blurring artifacts, which yields noisy images. In addition, the dynamic range of a sensor is usually defined by dividing the maximum achievable signal intensity by the maximum level of camera noise, and thus the sensor noise brings down the dynamic range. Simply taking into consideration the mean of multiple images with random errors can help reduce the amount of noise. Several authors have recently been investigating more effective integration techniques [2]–[9]. Buades et al. [2] proposed an effective method with sensor noise estimation for generating a noiseless and sharp image using multiple short exposure images or video. Mann and Picard [3] introduced a multiple exposure image integration technique for obtaining a noiseless high dynamic range (HDR) image. Matsuoka et al. [4] designed a weight function to further reduce the sensor and quantization noises in image integration, but it is not optimal in any sense. **Another weight optimization method [5] was proposed for image integration**, but the main purpose of this method is image-stitching, and they do not consider any restoration using multiple image denoising. On the other hand, several methods [6]–[9] can be used to effectively reduce the amount of noise using a noiseless flash image as a reference, but they are restricted

to using scenes where the flash light is fully reached.

Image super-resolution (SR) has also been widely investigated [10]–[15]. SR is the problem of recovering a high-resolution (HR) image from one or multiple low-resolution (LR) image inputs. Turkan et al. [14] introduced an effective single-image SR technique based on manifold learning. First, they estimate the optimal weights to approximate an input LR patch from its K nearest neighbors (K -NN) patches searching from the down-scaled images introduced from the input LR image, using locally linear embedding (LLE) [15]. Then, the HR patch is estimated using a weighted linear combination of the K -NN patches, which correspond to the K -NN patches in the LR patch space, based on the estimated weights in the HR patch space. They use scalar weights to reconstruct the HR patch, but it is much more difficult to reproduce the complex texture.

We propose a novel method for multiple image integration. The main contribution of the proposed method is that we find the optimal weight map using a convex optimization technique. In addition, we apply the proposed weight optimization scheme to the single-image SR problem. We show that the weight optimization significantly improves the capabilities of the denoising and super-resolution compared to some of the conventional approaches.

We explain the multiple image integration procedure, including the HDR acquisition, in the following section. In Sect.3, we introduce the method for the weight optimization. The problem is formulated as a convex optimization problem and the primal-dual splitting algorithm [16] is used to solve it. In Sect.4, we apply the proposed weight optimization scheme to an image SR problem. We demonstrate the validity of the proposed methods in Sect.5.

2. Multiple Image Integration

Let $\mathbf{u}_k \in \mathbb{R}^N$ ($k = 1, 2, \dots, K$) be the vectors representing the noisy observed images with N pixels. The multiple image integration can be expressed using the linear combination of the K weighted images $\mathbf{U}_k \mathbf{w}_k$, ($k = 1, 2, \dots, K$):

$$\mathbf{r} = \sum_{k=1}^K \mathbf{U}_k \mathbf{w}_k, \quad (1)$$

where $\mathbf{U}_k \in \mathbb{R}^{N \times N}$ is a $\{N \times N\}$ -diagonal matrix $\mathbf{U}_k = \text{diag}\{\mathbf{u}_k\}$, $\mathbf{w}_k \in \mathbb{R}^N$ is a weight map for \mathbf{u}_k , and $\mathbf{r} \in \mathbb{R}^N$ is an integrated image. The weight maps are normalized to $\sum_{k=1}^K \mathbf{w}_k = \mathbf{1}$,

Manuscript received January 1, 2011.

Manuscript revised January 1, 2011.

[†]The authors are with the Faculty of Environmental Engineering, the University of Kitakyushu, Fukuoka, 808–0135, Japan.

*This paper is partially based on the conference paper [1].

DOI: 10.1587/transinf.E0.D.1

where $\mathbf{1} \in \mathbb{R}^N$ is the vector of all ones, to preserve the energy of the image.

We need to compensate for the nonlinearity by estimating the inverse function f^{-1} of an in-camera intensity transform [17], [18] to accurately linearize the images in HDR image generation. We call the transform a "camera response curve" denoted by f in this paper that gives the relationship $\hat{\mathbf{u}}_k = f(\mathbf{u}_k \cdot t_k)$, where t_k is the exposure time of the k -th image, and $\hat{\mathbf{u}}_k, \mathbf{u}_k \in \mathbb{R}^N$ are the observed image and sensor output. If raw images are used or the image sensor has a linear sensitivity characteristic, this photometric calibration can be skipped. We adopted Mitsunaga et al.'s method [19] for among the calibration methods to estimate f^{-1} , in which the curve is approximated by a low order polynomial using multiple images and exposure ratios. Once the curve is estimated, the images are linearized by $\mathbf{u}_k = f^{-1}(\hat{\mathbf{u}}_k)/t_k$. The multiple exposure images when using our method are taken by varying the exposure times of a camera with other fixed settings. Then, the images are integrated using (1) to generate the HDR image.

3. Proposed Method

We need to find the denoised image \mathbf{r} and the weight \mathbf{w}_k with \mathbf{u}_k given in our framework. Finding the optimal values for the two variables inherently leads to an ill-posed and non-convex optimization problem. Thus, we start with the conventional weight in [20] as an initial guess, and then, construct \mathbf{r} using the method discussed in Sect.3.1. With the obtained image, we optimize the weight as explained in Sect.3.2. Finally, we again use the method in Sect.3.1 with the optimal weights to obtain a final result.

3.1 TV denoising

We adopt the conventional Total Variation denoising method [21] to find \mathbf{r} . Given the weight \mathbf{w}_k , the problem is defined as

$$\min_{\mathbf{r}} \left\| \sum_{k=1}^K \mathbf{U}_k \mathbf{w}_k - \mathbf{r} \right\|_2^2 + \lambda \|\mathbf{r}\|_{TV}, \quad (2)$$

where λ is the weight of the cost and $\|\cdot\|_{TV}$ is the anisotropic Total Variation regularization term. This minimization problem can be solved by using the *alternating direction method of multipliers* (ADMM) [22]. We iteratively perform two steps, solving a linear equation and conducting a shrinkage operation in the optimization procedure. Using the diagonalization by FFT and a soft-thresholding function, we can quickly obtain the solution (see [21] for more details).

3.2 Weight optimization for multiple image integration

The optimization for the weight \mathbf{w}_k is fulfilled by

$$\min_{\mathbf{w}} \|\bar{\mathbf{p}} - \mathbf{r}\|_2^2 + \alpha \|\mathbf{D}\bar{\mathbf{p}}\|_1$$

$$\text{s.t. } \sum_{k=1}^K \mathbf{w}_k = \mathbf{1}, \text{ and } \mathbf{w}_k \in C \ (k = 1, 2, \dots, K), \quad (3)$$

where α is the weight of the cost, $\bar{\mathbf{p}} = \sum_{k=1}^K \mathbf{U}_k \mathbf{w}_k$, $\mathbf{D} = [\mathbf{D}_h^T \ \mathbf{D}_v^T]^T \in \mathbb{R}^{2N \times N}$ are the vertically concatenated first-order differential operators in the horizontal $\mathbf{D}_h \in \mathbb{R}^{N \times N}$ and vertical $\mathbf{D}_v \in \mathbb{R}^{N \times N}$ directions, $(\cdot)^T$ stands for the transpose of (\cdot) , and a convex set C is defined as

$$C = \{\mathbf{x} \in \mathbb{R}^N \mid x_n \in [0, 1] \ (n = 1, 2, \dots, N)\}.$$

Owing to the weights satisfying $\sum_{k=1}^K \mathbf{w}_k = \mathbf{1}$, $\bar{\mathbf{p}}$ can be rewritten as

$$\bar{\mathbf{p}} = \sum_{k=1}^K \mathbf{U}_k \mathbf{w}_k = \sum_{k=1}^{K-1} (\mathbf{U}_k - \mathbf{U}_K) \mathbf{w}_k + \mathbf{u}_K = \mathbf{P}\mathbf{w} + \mathbf{u}_K, \quad (4)$$

where $\mathbf{P} \in \mathbb{R}^{N \times N(K-1)}$ and $\mathbf{w} \in \mathbb{R}^{N(K-1)}$ are denoted as

$$\mathbf{P} = [(\mathbf{U}_1 - \mathbf{U}_K) \ (\mathbf{U}_2 - \mathbf{U}_K) \ \dots \ (\mathbf{U}_{K-1} - \mathbf{U}_K)],$$

$$\mathbf{w} = [\mathbf{w}_1^T \ \mathbf{w}_2^T \ \dots \ \mathbf{w}_{K-1}^T]^T.$$

On the basis of the above discussion, the constrained problem of (3) is rewritten as an unconstrained problem:

$$\min_{\mathbf{w}} \|\mathbf{P}\mathbf{w} + (\mathbf{u}_K - \mathbf{r})\|_2^2 + \alpha \|\mathbf{D}(\mathbf{P}\mathbf{w} + \mathbf{u}_K)\|_1 + \iota_C(\mathbf{Q}\mathbf{w}) + \sum_{k=1}^{K-1} \iota_C(\mathbf{w}_k), \quad (5)$$

where ι_C denotes the indicator function,

$$\iota_C(\mathbf{x}) = \begin{cases} 0, & \text{if } \mathbf{x} \in C \\ +\infty, & \text{if } \mathbf{x} \notin C \end{cases}, \quad (6)$$

and $\mathbf{Q} \in \mathbb{R}^{N \times N(K-1)}$ is a $\{N \times N(K-1)\}$ -matrix composed of the $K-1$ identity matrices

$$\mathbf{Q} = \underbrace{[\mathbf{I}_N \ \mathbf{I}_N \ \dots \ \mathbf{I}_N]}_{K-1}. \quad (7)$$

The third term of (5) guarantees the solution satisfies $\sum_{k=1}^K \mathbf{w}_k = \mathbf{1}$ by taking into consideration $\mathbf{w}_K = \mathbf{1} - \sum_{k=1}^{K-1} \mathbf{w}_k$, and the fourth term forces \mathbf{w}_k to be within the $[0, 1]$ range.

The optimization problem in (5) is convex, and thus, can be solved by using the primal-dual splitting (PDS) algorithm [16]. The PDS algorithm solves the minimization problem of the form

$$\min_{\mathbf{x}} F(\mathbf{x}) + G(\mathbf{x}) + H(\mathbf{L}\mathbf{x}), \quad (8)$$

where F , G , and H are the proper, lower semi-continuous, and convex functions, and F is differentiable. \mathbf{L} is a linear operator. For the primal-dual algorithm to be applicable to our problem, we set

$$F(\mathbf{x}) = \|\mathbf{P}\mathbf{x} + (\mathbf{u}_K - \mathbf{r})\|_2^2, \\ G(\mathbf{x}) = 0,$$

$$\mathbf{L} = \begin{bmatrix} \text{---} & \text{DP} & \text{---} \\ \text{---} & \mathbf{Q} & \text{---} \\ \mathbf{I}_N & \mathbf{O} & \cdots & \mathbf{O} \\ \mathbf{O} & \mathbf{I}_N & \cdots & \mathbf{O} \\ \vdots & & \ddots & \vdots \\ \mathbf{O} & \mathbf{O} & \cdots & \mathbf{I}_N \end{bmatrix} \in \mathbb{R}^{(N(K+2)) \times (N(K-1))},$$

$$H(\mathbf{z}) = \alpha \|\mathbf{x}_a + \mathbf{g}\|_1 + \iota_C(\mathbf{x}_b) + \sum_{k=1}^{K-1} \iota_C(\mathbf{x}_{ck}),$$

$$\text{where } \mathbf{g} = \mathbf{D}\mathbf{u}_K \in \mathbb{R}^{2N},$$

$$\mathbf{x}_a = \mathbf{D}\mathbf{P}\mathbf{x} \in \mathbb{R}^{2N}, \mathbf{x}_b = \mathbf{Q}\mathbf{x} \in \mathbb{R}^N,$$

$$\mathbf{x} = [\mathbf{x}_{c1}^\top \mathbf{x}_{c2}^\top \cdots \mathbf{x}_{c(K-1)}^\top]^\top \quad (\mathbf{x}_{cs} \in \mathbb{R}^N) \text{ and}$$

$$\mathbf{z} = [\mathbf{x}_a^\top \mathbf{x}_b^\top \mathbf{x}^\top]^\top = \mathbf{L}\mathbf{x} \in \mathbb{R}^{N(K+2)}.$$

Then, the primal-dual splitting algorithm iteratively finds the two proximity operators[†]

1. $\mathbf{x}^{(\tau+1)} := \text{prox}_{\gamma_1 G}(\mathbf{x}^{(\tau)} - \gamma_1 \nabla F(\mathbf{x}^{(\tau)}) - \gamma_1 \mathbf{L}^* \mathbf{y}^{(\tau)})$
2. $\mathbf{y}^{(\tau+1)} := \text{prox}_{\gamma_2 H^*}(\mathbf{y}^{(\tau)} - \gamma_2 \mathbf{L}(2\mathbf{x}^{(\tau+1)} - \mathbf{x}^{(\tau)})),$ (9)

where ∇F is the gradient of F and \mathbf{L}^* is the adjoint of \mathbf{L} . The sequence $(\mathbf{x}^{(n)})_{n \in \mathbb{N}}$ weakly converges to the solution of (8) (see [16] for more details). The proximity operators in (9) are given by

$$\begin{aligned} \text{prox}_{\gamma_1 G}(\mathbf{x}) &= \mathbf{x}, \\ \text{prox}_{\gamma_2 H^*}(\mathbf{z}) &= \mathbf{z} - \gamma_2 \text{prox}_{H/\gamma_2} \left(\frac{\mathbf{z}}{\gamma_2} \right), \end{aligned} \quad (10)$$

where

$$\text{prox}_{H/\gamma_2}(\mathbf{z}) = [P_a(\mathbf{x}_a)^\top P_b(\mathbf{x}_b)^\top P_b(\mathbf{x}_{c1})^\top \cdots P_b(\mathbf{x}_{c(K-1)})^\top]^\top.$$

$P_a : \mathbb{R}^{2N} \rightarrow \mathbb{R}^{2N}$ is the soft-thresholding operator

$$P_a(x_n) = \begin{cases} x_n - \alpha/\gamma_2, & \text{if } x_n - \alpha/\gamma_2 > -g_n \\ x_n + \alpha/\gamma_2, & \text{if } x_n + \alpha/\gamma_2 < -g_n \\ -g_n, & \text{otherwise} \end{cases}, \quad (11)$$

where g_n is the n -th element of \mathbf{g} , and $P_b : \mathbb{R}^N \rightarrow \mathbb{R}^N$ is given by

$$P_b(x_n) = \begin{cases} 0, & \text{if } x_n < 0 \\ x_n, & \text{if } 0 \leq x_n \leq 1 \\ 1, & \text{if } x_n > 1 \end{cases}. \quad (12)$$

This discussion leads to Algorithm 1 shown below.

4. Image Super-Resolution using the weight optimization

Next, we apply the proposed weight optimization scheme

[†]The proximity operator for γ and $F(\mathbf{y})$ is defined as

$$\text{prox}_{\gamma F}(\mathbf{x}) = \arg \min_{\mathbf{y}} F(\mathbf{y}) + \frac{1}{2\gamma} \|\mathbf{x} - \mathbf{y}\|^2$$

Algorithm 1 Algorithm for solving (5)

- 1: Set $\tau = 0$ and $\mathbf{u}_k (k = 1, 2, \dots, K)$, $\mathbf{w}^{(0)}$ are given.
- 2: Solve (2) for $\mathbf{w} = \mathbf{w}^{(0)}$.
- 3: Set $\mathbf{x}^{(0)} = \mathbf{w}$, $\mathbf{y}^{(0)} = \mathbf{L}\mathbf{x}$.
- 4: $\mathbf{x}^{(\tau+1)} = \text{prox}_{\gamma_1 G}(\mathbf{x}^{(\tau)} - \gamma_1 \nabla F(\mathbf{x}^{(\tau)}) - \gamma_1 \mathbf{L}^* \mathbf{y}^{(\tau)})$
- 5: $\mathbf{y}^{(\tau+1)} = \text{prox}_{\gamma_2 H^*}(\mathbf{y}^{(\tau)} - \gamma_2 \mathbf{L}(2\mathbf{x}^{(\tau+1)} - \mathbf{x}^{(\tau)}))$
- 6: If the criterion is not satisfied, increment τ by 1 and then go back to 4.
- 7: Set $\mathbf{w} = \mathbf{x}^{(\tau+1)}$ and make an HDR image.
- 8: Solve (2)

to the super-resolution (SR) problem. The proposed SR method is based on the Turkan et al.'s SR method [14]. We will briefly summarize this algorithm first, and then, we will explain the details of the proposed SR approach.

4.1 The conventional SR algorithm

The SR algorithm in Turkan et al.'s method [14] is summarized as follows:

1. For each patch \mathbf{l}_i in the input LR image \mathbf{l} :
 - a. Find the K -nearest neighbors (K -NN) $\{\mathbf{v}_{i,k}^l\}_{k=1}^K$ of \mathbf{l}_i on the set of down-scaled images \mathcal{N}_{s_l} calculated from \mathbf{l} with a scaling factor of s_l .
 - b. Calculate the weights of the K -NN patches $\{\mathbf{v}_{i,k}^l\}_{k=1}^K$ that minimize the error from reconstructing \mathbf{l}_i .
 - c. Calculate the HR patch \mathbf{h}_i using the weights and the K -NN HR patches $\{\mathbf{v}_{i,k}^h\}_{k=1}^K$ corresponding to $\{\mathbf{v}_{i,k}^l\}_{k=1}^K$ (see Fig. 1).
 - d. If the estimated HR patch \mathbf{h}_i does not reach the desired scale, set $\mathbf{l}_i = \mathbf{h}_i$ and go back to Step 1a.
2. Construct the HR image \mathbf{h} using the simple weighted averaging of the stacked pixels with the overlapping patches, then applying the iterative back-propagation (IBP) [10] to preserve the global consistency between the HR image \mathbf{h} and the input LR image \mathbf{l} .

The SR using this method is achieved by gradually increasing the size of a given LR patch, e.g., by p -pixels in each dimension. This approach is based on the assumption that the small patch geometry can be preserved under small scaling factors [11]. The conventional method [14] calculates the scalar reconstruction weights of the K -NN patches in Step 1b. Due to the low degree of freedom, the results often have an over-smoothing effect and an unexpected artifact, especially when the target patch has a complex texture. Therefore, we use the proposed weight optimization scheme to improve these problems.

Figure 2 shows the flow of the proposed SR algorithm. In our method, the patches subtracted their mean energy, i.e., the SR approach handles the high frequency domain.

4.2 K -NN search

In the conventional method [14], the set of down-scaled images \mathcal{N}_{s_l} is introduced for searching the K -NN patches by down-scaling the input image \mathbf{l} with several pixel-shifting

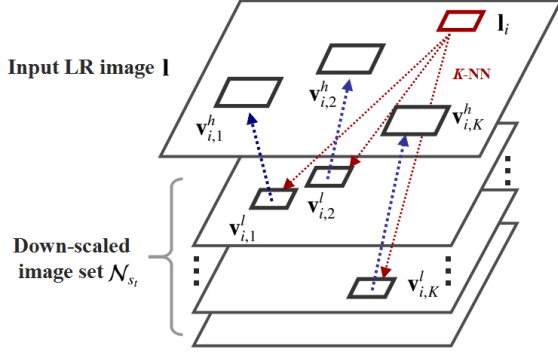
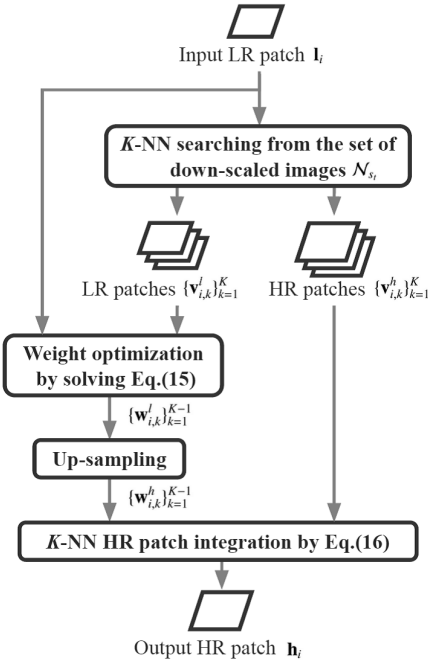

 Fig. 1 K -NN search from down-scaled images.


Fig. 2 Flow of proposed super-resolution.

offsets, where s_t is the down-scaling factor. Let the input LR patch size be $m \times m$ and the iteration number t (we set $t = 1$ as the initial value) in the Step 1. The down-scaling factor is obtained using $s_t = (m + (t-1)p)/(m + tp)$ by increasing pixel size p . Since this approach is inefficient and redundant, we introduce \mathcal{N}_{s_t} using several blurring kernels (four directional motion blur with 45 degree intervals from 0 to 135 degree, and Gaussian blur) and down-scaling to the input image \mathbf{l} , and search the K -NN patches. Note that we set the filter size to be the same as the target LR patch size. Let us denote LR and HR K -NN patch pairs as $\{v_{i,k}^l, v_{i,k}^h\}_{k=1}^K$.

4.3 Weight optimization for image super-resolution

We find the optimized weights for approximating the input LR patch by using the weighted linear combination of K -NN patches using LLE [15]. Then, we restore the unknown HR patch corresponding to the input LR patch by using the es-

timated weights. We propose the weight optimization problem, which is a slightly modified version of (3), to estimate the weights:

$$\begin{aligned} \min_{\hat{\mathbf{w}}_i^l} & \|\bar{\mathbf{p}}_i^l - \mathbf{l}_i\|_2^2 + \alpha \|\hat{\mathbf{D}}\hat{\mathbf{w}}_i^l\|_1 \\ \text{s.t.} & \sum_{k=1}^K \mathbf{w}_{i,k}^l = \mathbf{1}, \text{ and } \mathbf{w}_{i,k}^l \in C \ (k = 1, 2, \dots, K), \end{aligned} \quad (13)$$

where $\mathbf{l}_i \in \mathbb{R}^M$ is the target LR patch of the i -th pixel in the input LR image \mathbf{l} with M pixels, $\hat{\mathbf{w}}_i^l = [\mathbf{w}_{i,1}^{l\top} \ \mathbf{w}_{i,2}^{l\top} \ \dots \ \mathbf{w}_{i,K}^{l\top}]^\top \in \mathbb{R}^{MK}$ is a concatenated vector, which is composed of the weights $\mathbf{w}_{i,k}^l \in \mathbb{R}^M$ of K -NN patches $\mathbf{V}_{i,k}^l = \text{diag}\{v_{i,k}^l\} \in \mathbb{R}^{M \times M}$, and $\bar{\mathbf{p}}_i^l = \sum_{k=1}^K \mathbf{V}_{i,k}^l \mathbf{w}_{i,k}^l$. $\hat{\mathbf{D}} = \text{diag}\{\mathbf{D}', \mathbf{D}', \dots, \mathbf{D}'\} \in \mathbb{R}^{2MK \times 2MK}$ consists of the vertically concatenated first-order differential operators $\mathbf{D}' = [\mathbf{D}_h^\top \ \mathbf{D}_v^\top]^\top \in \mathbb{R}^{2M \times M}$ with horizontal $\mathbf{D}_h \in \mathbb{R}^{M \times M}$ and vertical operators $\mathbf{D}_v \in \mathbb{R}^{M \times M}$, and a convex set C is defined as

$$C = \{\mathbf{x} \in \mathbb{R}^M \mid x_n \in [0, 1] \ (n = 1, 2, \dots, M)\}.$$

The second term of (3) is introduced as a smoothness prior for an integrated image. The aim of super-resolution is to restore sharp edges by K -NN patch integration. For the purpose, we slightly modified the second term as a weight map smoothness prior in (13). This modified term induces the spatial smoothness to a weight map, and local consistency is preserved accordingly. Similar to (4), $\bar{\mathbf{p}}_i^l$ can be rewritten as

$$\bar{\mathbf{p}}_i^l = \sum_{k=1}^K \mathbf{V}_{i,k}^l \mathbf{w}_{i,k}^l = \sum_{k=1}^{K-1} (\mathbf{V}_{i,k}^l - \mathbf{V}_{i,K}^l) \mathbf{w}_{i,k}^l + \mathbf{v}_{i,K}^l = \mathbf{P}_i^l \mathbf{w}_i^l + \mathbf{v}_{i,K}^l, \quad (14)$$

where $\mathbf{P}_i^l \in \mathbb{R}^{M \times M(K-1)}$ and $\mathbf{w}_i^l \in \mathbb{R}^{M(K-1)}$ are denoted as

$$\begin{aligned} \mathbf{P}_i^l &= [(\mathbf{V}_{i,1}^l - \mathbf{V}_{i,K}^l) \ (\mathbf{V}_{i,2}^l - \mathbf{V}_{i,K}^l) \ \dots \ (\mathbf{V}_{i,K-1}^l - \mathbf{V}_{i,K}^l)], \\ \mathbf{w}_i^l &= [\mathbf{w}_{i,1}^{l\top} \ \mathbf{w}_{i,2}^{l\top} \ \dots \ \mathbf{w}_{i,K-1}^{l\top}]^\top. \end{aligned}$$

Furthermore, the constrained problem in (13) when introducing the indicator function ι_C , is rewritten as an unconstrained problem:

$$\begin{aligned} \min_{\mathbf{w}_i^l} & \|\mathbf{P}_i^l \mathbf{w}_i^l + (\mathbf{v}_{i,K}^l - \mathbf{l}_i)\|_2^2 + \alpha \|\hat{\mathbf{D}}\mathbf{w}_i^l\|_1 \\ & + \iota_C(\mathbf{Q}\mathbf{w}_i^l) + \sum_{k=1}^{K-1} \iota_C(\mathbf{w}_{i,k}^l), \end{aligned} \quad (15)$$

where $\mathbf{Q} \in \mathbb{R}^{M \times M(K-1)}$ is a $\{M \times M(K-1)\}$ -matrix composed of the $K-1$ identity matrices in (7). Here, we replaced the first-order differential block diagonal matrix $\hat{\mathbf{D}}$ of (13) with $\hat{\mathbf{D}} \in \mathbb{R}^{2M(K-1) \times 2M(K-1)}$, which are only different for the matrix dimension. The second term of (15) is introduced to add sparsity to the gradient of the weight map. The third term of (15) guarantees the solution satisfies $\sum_{k=1}^K \mathbf{w}_{i,k}^l = \mathbf{1}$ by taking $\mathbf{w}_{i,K}^l = \mathbf{1} - \sum_{k=1}^{K-1} \mathbf{w}_{i,k}^l$, and the fourth term forces $\mathbf{w}_{i,k}^l$ to be within the $[0, 1]$ range.

The cost function of (15) is also convex, and thus, can

be solved by using the PDS algorithm [16], which is described in Sect.3.2. For the PDS algorithm to be applicable to our problem in this SR problem, we set

$$F(\mathbf{x}) = \|\mathbf{P}_i^T \mathbf{x} + (\mathbf{v}_{i,K}^j - \mathbf{I}_i)\|_2^2,$$

$$G(\mathbf{v}) = 0,$$

$$\mathbf{L} = \begin{bmatrix} \text{---} & \tilde{\mathbf{D}} & \text{---} & \text{---} \\ \text{---} & \tilde{\mathbf{Q}} & \text{---} & \text{---} \\ \mathbf{I}_M & \mathbf{O} & \cdots & \mathbf{O} \\ \mathbf{O} & \mathbf{I}_M & \cdots & \mathbf{O} \\ \vdots & & \ddots & \vdots \\ \mathbf{O} & \mathbf{O} & \cdots & \mathbf{I}_M \end{bmatrix} \left(\in \mathbb{R}^{M(3K-2) \times M(K-1)} \right),$$

$$H(\mathbf{z}) = \alpha \|\mathbf{x}_a\|_1 + \iota_C(\mathbf{x}_b) + \sum_{k=1}^{K-1} \iota_C(\mathbf{x}_{ck}),$$

where $\mathbf{x}_a = \tilde{\mathbf{D}}\mathbf{x}$ ($\in \mathbb{R}^{2M(K-1)}$), $\mathbf{x}_b = \mathbf{Q}\mathbf{x}$ ($\in \mathbb{R}^M$),
 $\mathbf{x} = [\mathbf{x}_{c1}^T \ \mathbf{x}_{c2}^T \ \cdots \ \mathbf{x}_{c(K-1)}^T]^T$ ($\mathbf{x}_{cs} \in \mathbb{R}^M$) and
 $\mathbf{z} = [\mathbf{x}_a^T \ \mathbf{x}_b^T \ \mathbf{x}^T]^T = \mathbf{L}\mathbf{x}$ ($\in \mathbb{R}^{M(3K-2)}$).

According to the PDS algorithm, we iteratively find the two proximity operators in (9) (see Sect.3.2 for more details). Note that we set $g_n = 0$ for (11) in this SR problem. Thus, we solve it by using a similar procedure as described for Algorithm 1 without needing the image integration and the TV denoising.

Once the optimal weights $\{\mathbf{w}_{i,k}^j\}_{k=1}^{K-1}$ are obtained, we integrate the K -NN HR patches $\{\mathbf{v}_{i,k}^h\}_{k=1}^K$ by using them. Since there is a difference in the dimensions between the LR and HR patch pair, we obtain the up-sampled weights $\{\mathbf{w}_{i,k}^h\}_{k=1}^{K-1}$ by applying bicubic interpolation to the weights $\{\mathbf{w}_{i,k}^j\}_{k=1}^{K-1}$. Finally, the HR patch \mathbf{h}_i is obtained by

$$\mathbf{h}_i = \sum_{k=1}^{K-1} \mathbf{v}_{i,k}^h \mathbf{w}_{i,k}^h + \mathbf{v}_{i,K}^h. \quad (16)$$

Accordingly, we repeatedly perform the procedure while gradually expanding the patch size until the desired scaling factor s has been reached. Then, we reconstruct the target HR image \mathbf{h} by using the weighted averaging of the stacked pixels. In fact, the conventional method uses a uniform weight. Therefore, the reconstructed image is often over-smoothed. In contrast, we use non-uniform weights based on the Gaussian distribution, where the input is the distance between the center pixel and the others in each HR patch. Finally, we use the IBP method [10] to treat the estimated HR image \mathbf{h} to preserve the global consistency.

5. Experimental Results

We present and discuss our experimental results in this section. First, we discuss the multiple exposure image integration with denoising, and then, show the capability of the proposed weight optimization scheme by using it for the single-image SR problem.

Table 1 SNR and Nonlinear PSNR (NSNR), Hat: Hat function, Hat+TV: TV denoising with Hat function, and Our method.

Image	Hat		Hat+TV		Our method	
	SNR	NSNR	SNR	NSNR	SNR	NSNR
(a)	15.3	23.8	17.4	24.4	19.3	26.4
(b)	15.4	27.0	19.2	28.2	20.8	32.2
(c)	14.4	24.6	17.1	26.3	18.8	29.6

5.1 Multiple exposure image integration experiment

In the first experiment, we used several image sets with three different exposures to obtain HDR image, all of which were taken with ISO 100 sensitivity and had little noise. These shots were obtained by changing the shutter speed, while the aperture was fixed. **We simply integrate each image to a HDR image with a hat function and use it as a ground truth, which is commonly used for both of the conventional methods and ours.** We added white Gaussian noise to the images. We adopted the simple weight map in [20] and TV denoising in Sect.3.1, which is essentially same as [21], as the conventional methods we used for comparison.

The quantitative comparison is summarized in Table 1, in which we compare the proposed method with the weight of the hat function (Hat) in [20] and the TV denoising with the hat function (Hat+TV). Note that only the difference between Hat+TV and our method is the weights, and the same parameters are used in the TV denoising. For the quality metrics, we used the SNR[†] of the obtained HDR image and the nonlinear PSNR. The nonlinear PSNR is calculated by applying Reinhard et al.'s tone-mapping [17] to the HDR output to yield its low dynamic range version, and then, finding its PSNR. Since the HDR image contains a high dynamic range, the noises in its bright regions are overestimated by the SNR even though it is less perceivable than the noises in the shadows. The nonlinear PSNR may be a more suitable metric for evaluating HDR images when taking the human visual system into consideration. Images (a)-(c) in the list are shown as Figs.3(a)-(c). We can see from the results that the weight optimization significantly improves the image quality (see the parts circled in red).

In the second experiment, we took photographs with ISO 1600 sensitivity to obtain inputs with actual sensor noises, and then, applied the methods to them. Figures 3(d)-(e) illustrate the results for the images with actual sensor noises, which were taken with the ISO 1600 sensitivity. We averaged the fifteen photographs and the mean image is set as the ground truth. We can see from the figures that the conventional method (Hat+TV) sometimes had overly smooth edges, and especially lacked sufficient denoising for the bright region, while our method outperforms it.

The conventional weights such as the hat function play a role in eliminating the saturated pixels, while our method does not consider the pixel saturation. In our method, however, pixel saturation seldom occurs unless the input \mathbf{h} has

[†]Since the HDR image does not have a peak value, PSNR is not used for the comparison.

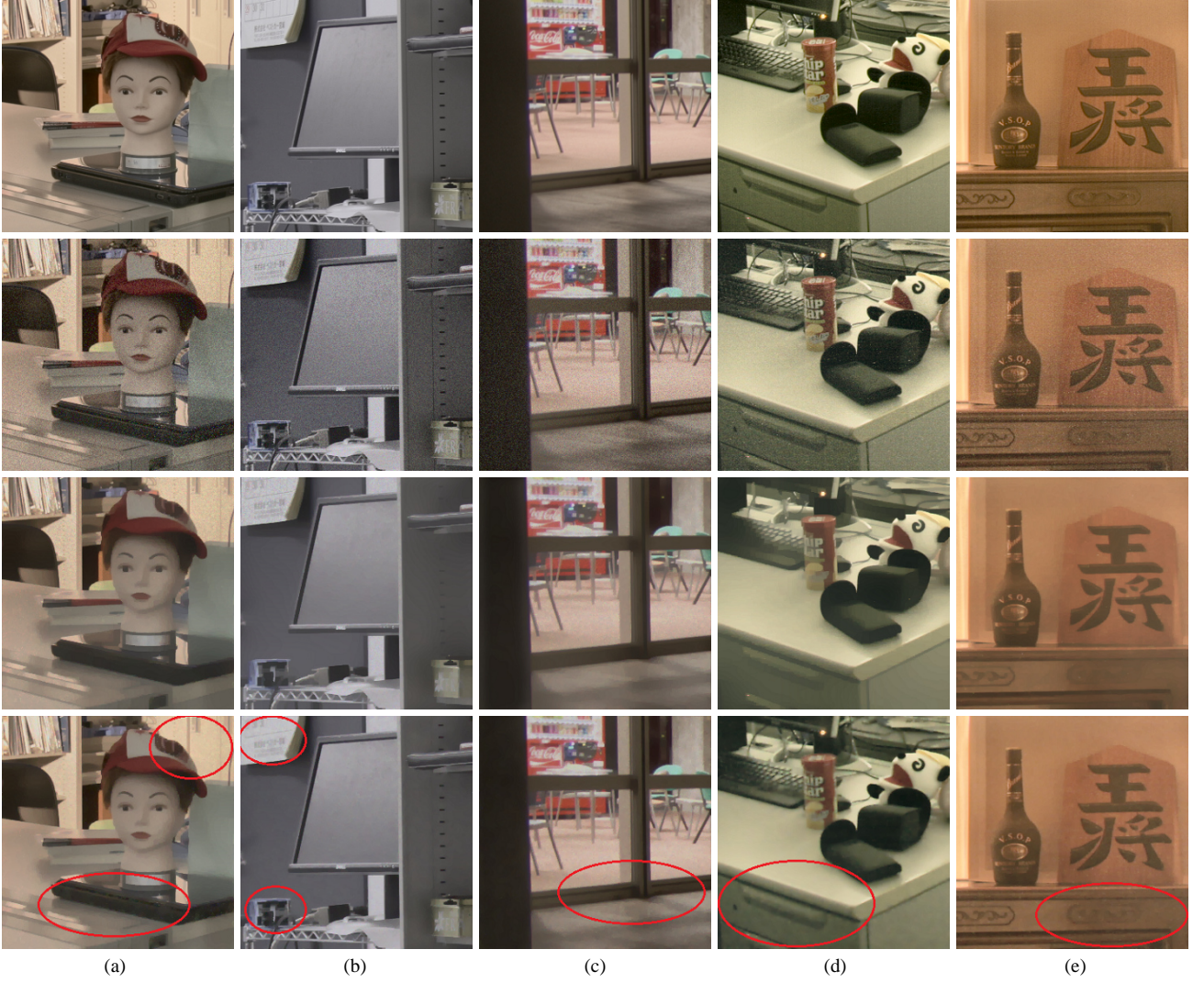


Fig. 3 Results: (from top to bottom) Ground truth, Simple hat function (Hat), Hat function plus TV (Hat+TV), and Our method. (a)-(c): images with AWGN, (d)-(e): images with actual sensor noise.

saturation by virtue of the first term of (3).

5.2 Single image-based super-resolution experiment

In this experiment, we compared our SR results with Turkan et al.'s SR method [14]. We set the SR factor $s=2$, the initial LR patch size $m=3$, and the increase size of patches $p=1$. The number of nearest neighbors was set to $K=8$ in our method. We used the parameter settings used in [14] for the conventional method.

We can see from the results shown in Fig.4 that the proposed method preserved the details of the scarf and knitwear better than the conventional method. Moreover, Fig.5 shows that the proposed method can restore the complex texture of the fur, particularly under the ear of the fox. The conventional method uses the scalar weight estimation for the approximation with the K -NN patches using LLE [15]. On the other hand, our method estimates the pixel-wise weights for the approximation with a high degree of freedom, to achieve

less approximation error and a better restoration than the conventional method.

Next, we show the validity of the proposed method by comparing the PSNR and SSIM [23] with that for the conventional method. We used two input images *Oldman* and *Fox* as the ground truth HR images, i.e., we used the down-scaled images of the input images with a factor of 2 as the input LR images, to calculate the PSNR and SSIM [23]. Table 2 itemizes the quantitative results of these scenes. The results show that our method outperforms the conventional method when comparing both the PSNRs and SSIMs [23].

We implemented the both weight optimization problems of the multiple exposure image integration and the super-resolution using Matlab on PC with Intel Core i7 2.4GHz CPU, 8GB RAM. For a 200×200 image, the multiple exposure image integration takes about 15 seconds. For a 132×100 image, the super-resolution takes about 20 minutes to finish our proposed algorithm on an average, while the conventional method [14] spends about 18 minutes.

Table 2 Comparison of PSNR and SSIM [23]

Image	Turkan et al. [14]		Proposed	
	PSNR	SSIM	PSNR	SSIM
<i>Oldman</i>	31.32	0.8781	32.92	0.9217
<i>Fox</i>	29.03	0.7688	29.20	0.7858

5.3 Parameter setting

The weight optimization problem has the parameter α in both of the cost functions (3) and (13), which determines the relative balance between the fidelity and the regularization terms. This is a user-defined parameter. The smoothness of the resulting image varies depending on this value. In the multiple exposure image integration experiments, we have set 0.8 and 1.2 to α for the case of the AWGN and the actual sensor noise, respectively. In the super-resolution experiment, we have set 10^{-4} to α . In our experiments, for both of the conventional and proposed methods, we have adjusted the parameter to yield the best possible quality after some trial-and-error for fair comparison.

6. Conclusion

We introduced a novel weight optimization scheme for multiple image integration in this paper. We proposed a weight optimization scheme with a TV denoising method to generate a noiseless HDR image. The estimated optimal weights, obtained by solving the proposed weight optimization problem using the PDS algorithm, can generate the noiseless HDR image from noisy input images. We have shown the validity of our method through our numerical simulations for the images with AWGN and actual sensor noises. The results showed that our method can reduce the noise in the dark and bright regions more than when using the others, while maintaining the details of the scene.

Additionally, as an application of the proposed weight optimization scheme, we introduced the single-image SR method based on the proposed pixel-wise weight optimization. In this application, a HR image can be restored from the weighted linear combination of K -NN patches with the optimal weights, which are obtained by solving the proposed weight optimization problem in the LR patch space and using simple up-sampling. The qualitative and quantitative experimental results showed that the proposed method achieved better restoration results than the conventional method when using the pixel-wise weight optimization scheme.

Acknowledgments

This work was supported in part by JSPS Grants-in-Aid (24560473) and the KDDI foundation.

References

- [1] R. Matsuoka, T. Yamauchi, T. Baba, and M. Okuda, "Weight optimization for multiple image integration," *Image Processing (ICIP)*,



(a) Turkan et al. [14] (b) Proposed method

Fig. 4 Super-resolution results for *Oldman* with close-ups.

(a) Turkan et al. [14] (b) Proposed method

Fig. 5 Super-resolution results for *Fox* with close-up.

- [2] 2013 20th IEEE International Conference on, pp.795–799, Sept 2013.
- [2] Mann, Picard, S. Mann, and R.W. Picard, "On being 'undigital' with digital cameras: Extending dynamic range by combining differently exposed pictures," *Proceedings of IS&T*, pp.442–448, 1995.
- [3] T. Buades, Y. Lou, J. Morel, and Z. Tang, "A note on multi-image denoising," *Local and Non-Local Approximation in Image Processing*, 2009. LNLA 2009. International Workshop on, pp.1–15, Aug 2009.
- [4] R. Matsuoka, T. Jinno, and M. Okuda, "Multiple exposure integration with image denoising," *Signal Information Processing Association Annual Summit and Conference (APSIPA ASC)*, 2012 Asia-Pacific, pp.1–4, Dec 2012.
- [5] W. Wang and M. Ng, "A variational method for multiple-image blending," *Image Processing, IEEE Transactions on*, vol.21, no.4, pp.1809–1822, April 2012.

- [6] G. Petschnigg, R. Szeliski, M. Agrawala, M. Cohen, H. Hoppe, and K. Toyama, "Digital photography with flash and no-flash image pairs," *ACM Trans. Graph.*, vol.23, no.3, pp.664–672, Aug. 2004.
- [7] K. Shirai, M. Okamoto, and M. Ikehara, "Noiseless no-flash photo creation by color transform of flash image," *Image Processing (ICIP)*, 2011 18th IEEE International Conference on, pp.3437–3440, Sept 2011.
- [8] R. Matsuoka, T. Baba, M. Okuda, and K. Shirai, "High dynamic range image acquisition using flash image," *Acoustics, Speech and Signal Processing (ICASSP)*, 2013 IEEE International Conference on, pp.1612–1616, May 2013.
- [9] T. Baba, R. Matsuoka, S. Ono, K. Shirai, and M. Okuda, "Flash/no-flash image integration using convex optimization," *Acoustics, Speech and Signal Processing (ICASSP)*, 2014 IEEE International Conference on, pp.1185–1189, May 2014.
- [10] M. Irani and S. Peleg, "Motion analysis for image enhancement: Resolution, occlusion, and transparency," *Journal of Visual Communication and Image Representation*, vol.4, pp.324–335, 1993.
- [11] W. Freeman, T. Jones, and E. Pasztor, "Example-based super-resolution," *Computer Graphics and Applications, IEEE*, vol.22, no.2, pp.56–65, Mar 2002.
- [12] S. Farsiu, M. Robinson, M. Elad, and P. Milanfar, "Fast and robust multiframe super resolution," *Image Processing, IEEE Transactions on*, vol.13, no.10, pp.1327–1344, Oct 2004.
- [13] M. Türkan, D. Thoreau, and P. Guillotel, "Self-content super-resolution for ultra-hd up-sampling," *Proceedings of the 9th European Conference on Visual Media Production, CVMP '12*, New York, NY, USA, pp.49–58, ACM, 2012.
- [14] M. Turkan, D. Thoreau, and P. Guillotel, "Optimized neighbor embeddings for single-image super-resolution," *Image Processing (ICIP)*, 2013 20th IEEE International Conference on, pp.645–649, Sept 2013.
- [15] S.T. Roweis and L.K. Saul, "Nonlinear dimensionality reduction by locally linear embedding," *Science*, vol.290, no.5500, pp.2323–2326, December 2000.
- [16] L. Condat, "A primal-dual splitting method for convex optimization involving Lipschitzian, proximable and linear composite terms," *Journal of Optimization Theory and Applications*, vol.158, no.2, pp.460–479, 2013.
- [17] E. Reinhard, G. Ward, S. Pattanaik, and P. Debevec, *High Dynamic Range Imaging: Acquisition, Display, and Image-Based Lighting (The Morgan Kaufmann Series in Computer Graphics)*, Morgan Kaufmann Publishers Inc., San Francisco, CA, USA, 2005.
- [18] T. Jinno and M. Okuda, "Multiple exposure fusion for high dynamic range image acquisition," *Image Processing, IEEE Transactions on*, vol.21, no.1, pp.358–365, Jan 2012.
- [19] T. Mitsunaga and S. Nayar, "Radiometric self calibration," *Computer Vision and Pattern Recognition, 1999. IEEE Computer Society Conference on.*, pp.–380 Vol. 1, 1999.
- [20] P.E. Debevec and J. Malik, "Recovering high dynamic range radiance maps from photographs," *Proceedings of the 24th Annual Conference on Computer Graphics and Interactive Techniques, SIGGRAPH '97*, New York, NY, USA, pp.369–378, ACM Press/Addison-Wesley Publishing Co., 1997.
- [21] Y. Wang, J. Yang, W. Yin, and Y. Zhang, "A new alternating minimization algorithm for total variation image reconstruction," *SIAM J. Img. Sci.*, vol.1, no.3, pp.248–272, Aug. 2008.
- [22] D. Gabay and B. Mercier, "A dual algorithm for the solution of nonlinear variational problems via finite element approximation," *Computers & Mathematics with Applications*, vol.2, no.1, pp.17 – 40, 1976.
- [23] Z. Wang, A. Bovik, H. Sheikh, and E. Simoncelli, "Image quality assessment: from error visibility to structural similarity," *Image Processing, IEEE Transactions on*, vol.13, no.4, pp.600–612, April 2004.

**Ryo Matsuoka****Tomohiro Yamauchi****Tatsuya Baba****Masahiro Okuda**